Nanoscale

Cite this: *Nanoscale*, 2012, **4**, 5461

www.rsc.org/nanoscale

PAPER

Cell "vision": complementary factor of protein corona in nanotoxicology†

Morteza Mahmoudi,*[abc] Seyyed N. Saeedi-Eslami,[c] Mohammad A. Shokrgozar,[c] Kayhan Azadmanesh,[d] Maryam Hassanlou,[c] Hamid R. Kalhor,[e] Carmen Burtea,[f] Barbara Rothen-Rutishauser,[g] Sophie Laurent,[f] Sara Sheibani[h] and Hojatollah Vali[h]

Received 14th May 2012, Accepted 20th June 2012
DOI: 10.1039/c2nr31185b

Engineered nanoparticles are increasingly being considered for use as biosensors, imaging agents and drug delivery vehicles. Their versatility in design and applications make them an attractive proposition for new biological and biomedical approaches. Despite the remarkable speed of development in nanoscience, relatively little is known about the interaction of nanoscale objects with living systems. In a biological fluid, proteins associate with nanoparticles, and the amount and the presentation of the proteins on their surface could lead to a different *in vivo* response than an uncoated particle. Here, in addition to protein adsorption, we are going to introduce concept of cell "vision", which would be recognized as another crucial factor that should be considered for the safe design of any type of nanoparticles that will be used in specific biomedical applications. The impact of exactly the same nanoparticles on various cells is significantly different and could not be assumed for other cells; the possible mechanisms that justify this cellular response relate to the numerous detoxification strategies that any particular cell can utilize in response to nanoparticles. The uptake and defence mechanism could be considerably different according to the cell type. Thus, what the cell "sees", when it is faced with nanoparticles, is most likely dependent on the cell type.

1 Introduction

In the context of several scientific reports showing the potential risks of a rapidly growing new field of science, such as nanotechnology, there have been some novels that present a malicious view about the future of nanotechnology, among which Michael Crichton's *Prey* is noteworthy.[1,2] Such a trend vividly suggests that not only scientists are worried about the future of nanotechnology, but ordinary people may also have similar concerns. Indeed, there are few technical reports on the cytotoxicity of nanoparticles (NPs) (Definition for a NP; a nano-object [a material with one, two or three external dimensions in the nanoscale (1–100 nm)] with all three external dimensions in the nanoscale)[3] but instead consist of synthetic routes for obtaining NPs, creating a significant gap between a deep understanding of NP toxicity *versus* nanomaterial properties.[4–6] Hence, it is too difficult to predict the exact future risks and consequences from their qualities/quantities.

Since NPs are small enough to enter almost all areas of the body such as organs, tissues, cells and organelles, they carry a great potential as a new approach to conventional medicine so called "nanomedicine".[7,8] Dawson's group introduced the innovative idea on NP toxicity in 2007;[9,10] they focused on introducing a new interface called "bio-nano" interface. More specifically, they showed that when nanoparticles enter a biological environment, the nanoparticles become coated with various amounts of proteins that may transmit biological effects, such as accumulation of NPs in liver and in spleen due to the opsonin protein absorption at the surface of NPs.[11] Indeed, the resulting changes in protein conformation and/or avidity effects arising from the close spatial repetition of the same proteins.[10] In addition, when cells are exposed to NPs, the cellular proteins tend to become fibrillated (amyloid-like); the fibrillation may have significant effects on induction/propagation of neurodegenerative diseases such as Parkinson's.[12] In order to achieve a deep understanding of the biological effects of NPs, one requires knowledge of the equilibrium and kinetic binding properties of proteins/biomolecules that associate with the particles. A number

[a]*Department of Nanotechnology, Faculty of Pharmacy, Tehran University of Medical Sciences, Tehran, Iran; Web: www.biospion.com. E-mail: Mahmoudi@biospion.com; Mahmoudi-m@TUMS.ac.ir*
[b]*Nanotechnology Research Centre, Faculty of Pharmacy, Tehran University of Medical Sciences, Tehran, Iran*
[c]*National Cell Bank, Pasteur Institute of Iran, Tehran, Iran*
[d]*Virology Department, Pasteur Institute of Iran, Tehran, 1316943551 Iran*
[e]*Biochemistry Research Laboratory, Department of Chemistry, Sharif University of Technology, P. O. Box 11365-9516, Tehran, Iran*
[f]*Department of General, Organic, and Biomedical Chemistry, NMR and Molecular Imaging Laboratory, University of Mons, Avenue Maistriau, 19, B-7000 Mons, Belgium*
[g]*Adolphe Merkle Institute, Université de Fribourg, CH-1723 Marly, Switzerland*
[h]*Dept. of Earth & Planetary Sciences/Department of Anatomy & Cell Biology, McGill University, Montréal, Québec, Canada*
† Electronic supplementary information (ESI) available. See DOI: 10.1039/c2nr31185b

of recent publications were dedicated to this issue, attesting to its importance.[13–15]

In the present study, we put forward a perspective, which is vital to the cell-NPs interaction; we coined this perspective "cell vision". Recent exciting findings have confirmed that the biological environment is dynamic and intelligent enough to comprehend the induction of external stimulation even when the induction is at the nanoscale level. For instance, cells can actively control the NP dose across a cell population.[16,17] Thus, the "cell vision" is quite important as a crucial issue for designing and engineering the surface of NPs for specific biological applications; otherwise, the optimized effect of NPs would be significantly decreased. In fact, it has been fairly well-understood that asymmetric cell division has been developed as an evolutionary safety mechanism for ensuring that potential toxins, *e.g.* damaged proteins, are preferentially inherited by one of the daughter cells upon division;[17] more specifically, one of the daughters becomes the sole cell carrying the materials potentially damaging to the cell, resulting in the maintenance of the health of the wider cell population.[16,17] Therefore, if the NPs are prepared to deliver drugs to specific cells, the corresponding cell division asymmetry could negate this specificity by dispersing the drug dose during cell proliferation; it is notable that predetermined cell proliferation is highly related to the cell type. In addition to the importance of the "cell vision" in accelerating the nanosystem design, the cytotoxicity evaluations of NPs could be highly dependent on the "cell vision". Based on the scientific literature, where a growing number of papers have explored the cytotoxicity of NPs,[18–28] it has been suggested that there could be significant differences in the cytotoxicity among different cell lines treated with identical concentrations of the same NPs. Therefore, the obtained cytotoxicity data is reliable for the examined cells only and cannot be generalized for other cell lines.

We claim that the dynamic and intelligent role of the cells are highly related to their type and their "vision"; consequently, a deep understanding of the proposed "cell vision", would create a great opportunity for the nanomedicine community to identify suitable nano-systems in order to offer safe and positive effects for satisfying the desired purposes with very high yields.

In the present work, we have examined the effects of the same concentrations of superparamagnetic iron oxide nanoparticles (SPIONs) on several cell lines of different origin. It is noteworthy that among the various NPs employed in biomedical engineering, SPIONs have been selected as model NPs due to their multi-modality and multi-tasking abilities along with their excellent biocompatibility.[29,30] The selected cell lines include cells from liver, spleen, cervix epithelium, lung, connective tissue, colon, brain (neuronal and glial cells), skin, pancreas, and myocardium (see Table 1). Using the various cell lines, we compared the type of responses that the cells would display to the same NPs, at the cellular level (*e.g.*, MTT, and XTT) and at the molecular level (*e.g.* microarray).

Our results support the notion that the same NPs trigger different responses and mechanisms in different cell types. Therefore, it is crucial for scientists to consider "cell vision" as an approach for achieving a more effective design and usages of their desired NPs.

2 Materials and methods

2.1 Cell culture and treatments

Various cell lines from different origins (*e.g.* brain, heart, lung, liver, skin, kidney, colon, and cervix) have been used for the cytotoxicity assays. The employed cells are described in Table 1. Panc-1 and Capan-2 cells were kindly offered by Dr Daizy Flamez (Free University of Brussels, Experimental Medicine Laboratory, Belgium). Panc-1 cells were cultured in pyruvate-free DMEM culture medium (Lonza, Verviers, Belgium) supplemented with 10% fetal bovine serum, non-essential amino acids (both from Invitrogen), and penicillin/streptomycin (Lonza). Capan-2 cells were cultured in advanced RPMI-1640 culture medium supplemented with 10% fetal bovine serum, glutamax (all from Invitrogen), and penicillin/streptomycin (Lonza). Jurkat cells (gift from Prof. Oberdan Leo, Free University of Brussels, IBMM, Belgium) were cultured at a concentration of less than 1×10^6 cells per ml in RPMI-1640 culture medium (Sigma-Aldrich, Bornem, Belgium) supplemented with 10% heat inactivated newborn calf serum and antibiotic–antimycotic (both from Invitrogen). HeLa cells were cultured in MEM culture medium supplemented with 10% fetal calf serum, glutamax, antibiotic–antimycotic, non-essential amino acids, and sodium pyruvate (all from Invitrogen). Other cells were prepared from the National Cell Bank of Iran (NCBI), Pasteur Institute of Iran and their specific mediums are presented in Table 1.

2.2 MTT and XTT assays

All cell lines were seeded into flat-bottom 96-well culture plates at a density of 10 000 cells (2500 cells for HCM cell line) per well in 100 μl of medium. After 24 h, 40 μl of the corresponding medium containing various concentrations of SPIONs (2–32 mM) was added to each well. Forty μl of base medium for each cell line was added to negative control wells. All specimens as well as controls were placed in 5 wells to provide statistically reliable results. The cells were cultured in their specific mediums (see Table 1) and maintained at 37 °C in a 5% or 10% CO_2 incubator.

Cytotoxicity was assessed using the MTT (3-(4,5-dimethylthiazol-2-yl)-2,5-diphenyltetrazolium bromide) and XTT (sodium(2,3-bis(2-methoxy-4-nitro-5-sulphophenyl)-2*H*-tetrazolium-5-carboxanilide)) assays, which are non-radioactive, colorimetric techniques. Considering the MTT assay, 24 h after the incubation with SPIONs, 100 μl of MTT (0.5 mg ml^{-1}) was added to each well. Following incubation, the medium was removed and formazan crystals were solubilized by incubation for 20 min in 150 μl of isopropanol. The absorbance of each well, which assesses viable cells, was read at 545 nm on a microplate reader (Stat Fax-2100, AWARENESS, Palm City, USA). Regarding the XTT assay, 24 h after the incubation with SPIONs, 50 μl of XTT labeling mixture was added to each well and incubated for 18 h, after that the amount of formazan crystals were measured using a plate reader. For the MTT and XTT studies, all experiments were carried out in triplicate (*i.e.* three 96 plates; total 15 repeats) with the results expressed as mean ± standard deviation; standard deviation values are indicated as error bars in the relevant MTT plots. The results were statistically processed for outlier detection using a "T procedure"

Table 1 Description of the cell lines used in MTT and XTT studies (DMEM: Dulbecco's modified Eagle's medium; Ham's: Nutrient Mixture F-10; FBS: fetal bovine serum; RPMI-1640 (Roswell Park Memorial Institute))

Cell code	Cell type	Culture medium
BE(2)-C	Human neuroblastoma	1 : 1 (DMEM + Ham's F12) + FBS10%
A172	Human glioblastoma	DMEM + FBS10%
HCM	Human cardiac myocytes	1 : 1 (DMEM + Ham's F12) + FBS10% supplemented with 5 μg ml^{-1} insulin and 50 ng ml^{-1} bFGF
A549	Human lung adenocarcinoma	DMEM + FBS10%
HepG2	Human hepatocellular carcinoma	RPMI 1640 + FBS10%
A-431	Human epithelial carcinoma	DMEM + FBS10%
293T	Human embryonic kidney	RPMI 1640 + FBS10%
SW480	Human colon adenocarcinoma	DMEM + FBS10%
HeLa	Human cervical adenocarcinoma	MEM + FBS10%
Capan-2	Human pancreas adenocarcinoma	RPMI + FBS10%
Panc-1	Human pancreatic carcinoma	DMEM + FBS10%
Jurkat	Human T cell lymphoblast-like	RPMI + FBS10%
L929	Mouse connective tissue fibroblast	RPMI + FBS10%

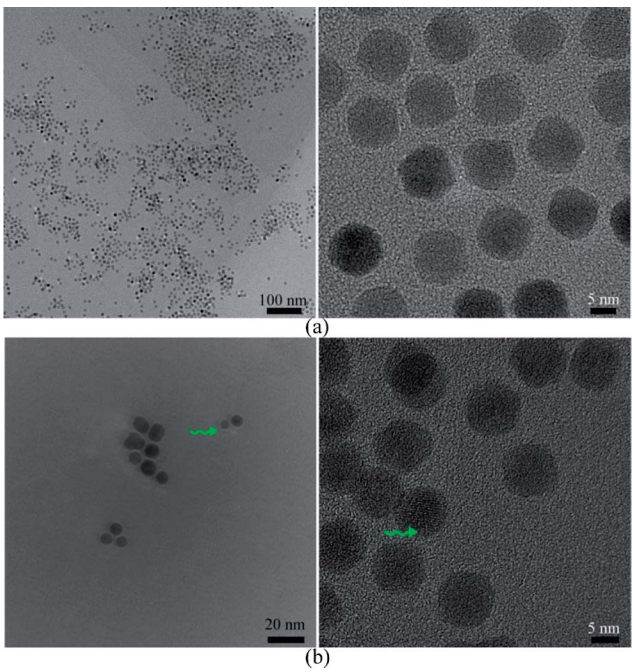

Fig. 1 TEM image of (a) bare and (b) polymer coated monodisperse iron oxide nanocrystals (arrows show the coating materials).

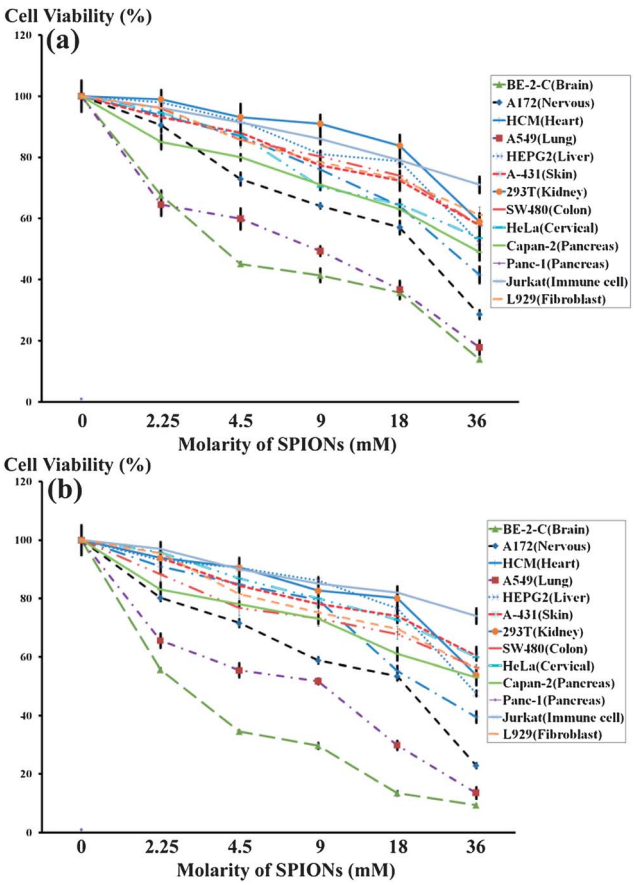

Fig. 2 Cells viabilities of (a) MTT- and (b) XTT-assay results after treatment with various concentrations of SPIONs.

in the MINITAB software (Minitab Inc., State College, PA).[31] Statistical differentiations were made by one-way analyses of variance (ANOVA), for which $p < 0.05$ was considered as statistically significant. It is notable to mention that the interaction of the SPIONs with the assay dyes were probed to ensure that there is no binding between them.

2.3 Reactive oxygen species (ROS) assays

For visualization by confocal microscope, the adherent cells (Panc-1, Capan-2, and HeLa) were seeded on coverslips before incubating with various compounds, while Jurkat cells were incubated in suspension. The cells were incubated for 24 h with 55.845 μg iron per ml (1 mM of iron) that was added to the culture medium. Control cells were not incubated with SPIONs. The cells were then washed three times with ice-cold PBS and incubated for 1 h with 10 mM 5-(and-6)-chloromethyl-2,7-dichlorodihydrofluorescein diacetate acetyl ester (H_2DCFDA, Invitrogen, Merelbeke, Belgium) in PBS (10%) at 37 °C. The cells were subsequently washed three times with ice-cold PBS, fixed with 2% paraformaldehyde for 15 min at room temperature and the cell-coated coverslips were finally mounted on microscope

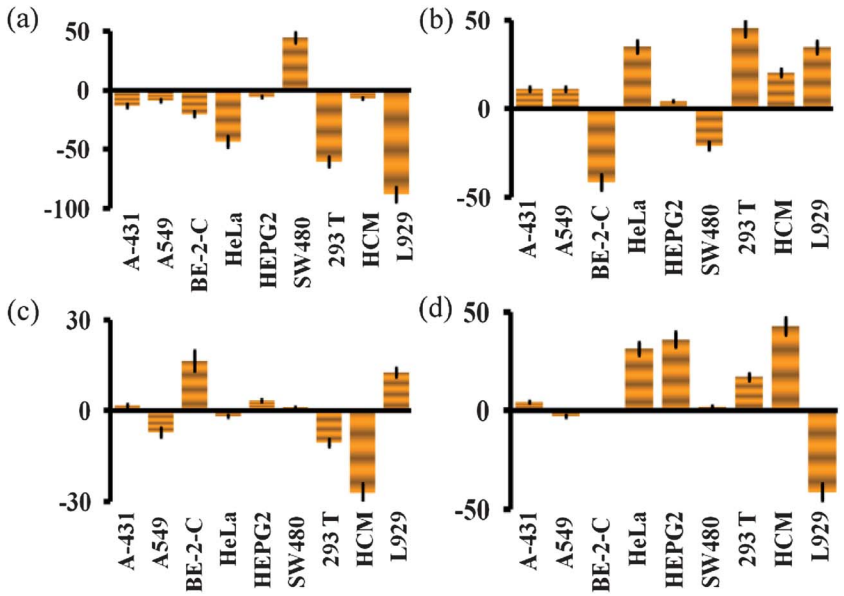

Fig. 3 Cell-life cycle assay results for SPIONs-treated cells showing the percentage of (a) (sub G_0G_1(control) − subG_0G_1(test))/subG_0G_1(control), (b) (G_0G_1(control) − G_0G_1(test))/G_0G_1(control), (c) (S(control) − S(test))/S(control), and (d) (G_2(control) − G_2(test))/G_2(control) for A-431, A549, BE-2-C, HeLa, HepG2, SW480, 293 T, HCM, L929, Panc-1, Capan-2, and jurkat cell lines, respectively.

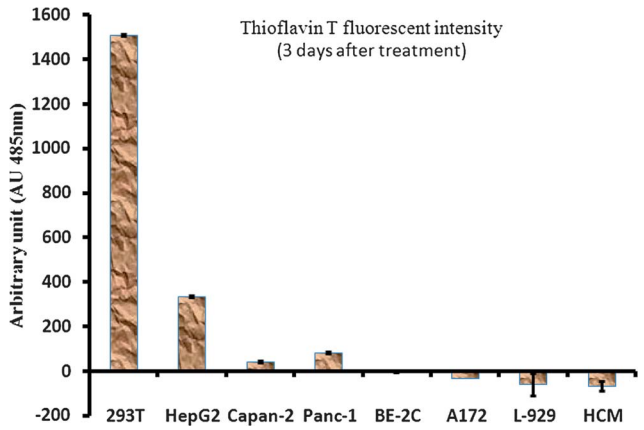

Fig. 4 Amyloid formation in the presence of nanoparticles. Various cell lines were exposed to the same nanoparticle concentration (2 mM). After 3 days, the Thioflavin T fluorescence was measured as explained in the Experimental section.

slides by using Vectashield mounting medium with DAPI (Vector Labconsult, Brussels, Belgium).[32] The method of ROS labeling was slightly modified for Jurkat cells, which grow in suspension. The cells (2×10^6 ml^{-1}) were incubated (45 min, 37 °C) with 25 μM H_2DCFDA in HBSS. Five min before ending the incubation with H_2DCFDA, a solution of Hoechst 33342 dye was added at a final concentration of 1 μM. The cells were then rinsed three times with HBSS, the supernatant being removed by centrifugation. At the end, the cells were mounted on microscope slides after resuspending them in 25 μl HBSS. All the samples were observed on a confocal microscope. A semi-quantitative analysis of the microscope pictures was performed using the ImageJ image analysis software, the fluorescence intensities being related to the cell number per picture. The results were expressed as percentage of cell labeling in SPION-treated samples as compared to control cells.

2.4 Lysosome labeling

Panc-1, Capan-2, Jurkat, and HeLa cells were labeled with Image-iT™ LIVE lysosomal and nuclear labeling kit (Molecular Probes, Invitrogen), which provides a red-fluorescent Lyso-Tracker® Red DND-99 dye for lysosome staining, and a blue-fluorescent Hoechst 33342 dye for staining the nucleus. The adherent cells (Panc-1, Capan-2, and HeLa) were seeded on coverslips before incubating with various compounds. Jurkat cells, which are not adherent, were incubated in suspension, the various compounds being removed by centrifugation. The cells were incubated (37 °C, 24 h) with SPIONs that were added in the culture medium at a concentration of 55.845 μg ml^{-1} (1 mM of iron). Control cells were not incubated with SPIONs. After rinsing the cells with Hanks Buffered Salt Solution (HBSS), they were labeled with Image-iT™ LIVE lysosomal and nuclear labeling kit according to the supplier's instructions. Briefly, the cells were incubated for 5 min with 2 μg ml^{-1} of Hoechst 33342 solution, followed by 1 min incubation with 100 nM of Lyso-Tracker Red DND-99®. The cells were rinsed two times with HBSS after each dye. The living cells were finally mounted in HBSS on microscope slides and observed on a DM2000 Leica microscope (Leica Microsystems, Groot Bijgaarden, Belgium), the pictures being acquired with a Leica DFC 290 camera. The microscope pictures were finally analyzed using the ImageJ software, as described above.

2.5 Crystal violet staining

The cell culture medium was removed carefully from the wells and the cells washed gently with PBS warmed to room

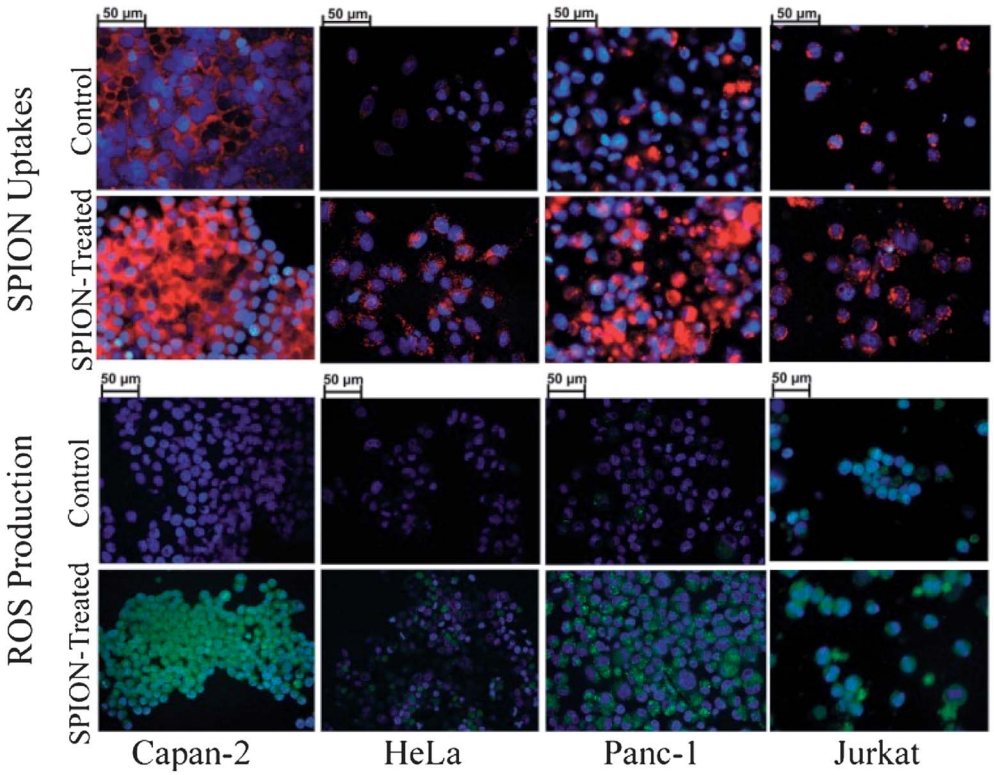

Fig. 5 Induced lysosomes in (a) Capan-2, (b) Panc-1, (c) Hela, and (d) Jurkat cells obtained by their interactions with SPIONs. In a live lysosome assay, the lysosomes and nucleus are seen as red and blue fluorescence, respectively. Induced ROS levels in (e) Capan-2, (f) Panc-1, (g) Hela, and (h) Jurkat cells obtained by their interactions with SPIONs. In intracellular ROS assays, the ROS level and nucleus are seen as green and blue fluorescence, respectively.

temperature. One hundred μl of a crystal violet solution (containing 0.5% Crystal Violet), 20% methanol 20 μl, distilled H_2O 80 μl) was added to the cells, incubated for 10 minutes at room temperature, and washed off with PBS before imaging.

2.6 Cell cycle assay

Cell cycle assay was carried out by staining of the DNA with Propidium Iodide (PI) followed by flow cytometric measurement of the fluorescence. Approximately 10^6 cells of each cell line were maintained in culture after defreezing, to retain their physiologic cell cycle distribution. After achieving 75% confluence they were treated with the same amount of SPIONs (*i.e.* 2 mM) for 24 h. The adhering cells were detached from the plates by trypsine + EDTA or EDTA alone (25 mg trypsin and 5 mg EDTA per 1cc) and harvested. The obtained suspensions of adhering or floating cells were centrifuged at 280 g. The collected cells were washed with PBS a couple of times at 200 g. The cells have been thoroughly resuspended in PBS by Pasteur pipette in order to have a monodisperse cell suspension at the time of mixing cells with ethanol. Cells were fixed in ethanol *via* transferring into the tubes containing 70% ethanol and stored in −20 °C for several days. Prior to the flow cytometric analysis, the ethanol-suspended cells were centrifuged at 300 g for 5 min and the supernatants were decanted thoroughly. The collected cells were washed with PBS and then suspended in 1 ml of PI/Triton X-100 staining solution with 100 μg ml^{-1} of RNase A, followed by keeping at 37 °C for 30 min. The stained cells were then analyzed by flow cytometry using a Cyflow SL machine (Partec, Germany) with excitation at 488 nm and collecting data at FL2. The readings were analyzed with Flowjo software (Treestar Inc., CA, USA).

2.7 Assessment of amyloid formation

The assay for the presence of amyloid was done as previously reported[33] with some modifications. Briefly, in 96-well tissue culture plates, various cell lines were grown to near confluence and the cells incubated in the absence or presence of the SPIONs at 25 mM final concentration in culture medium. After 3 days, the cells were rinsed three times with PBS and were fixed with 3% paraformaldehyde in PBS for 20 min. Afterwards, the samples were incubated with RNase A, in PBS at a concentration of 50 μg ml^{-1}, for 20 min to remove cellular RNA. The cells were then rinsed with PBS and stained with 0.1% thioflavin T for 10 min. Following this, the cells were rinsed with 80% ethanol three times. Two hundred and fifty ml of PBS was added to each well, and thioflavin T fluorescence was measured at an excitation wavelength of 440 nm and an emission wavelength of 485 nm using the Synergy 4 fluorescence plate reader (BioTek, USA). Each measurement was performed in quadruplicates. The quantification for thioflavin T was done based on the below equation:

$$[(A_1 - A_2) - (B_1 - B_2)]/(B_1 - B_2) \quad (1)$$

Whereas A_1 is cells that are exposed to NPs and stained with Thioflavin T, A_2 is cells that are exposed to NPs and without staining with nanoparticle, B_1 is cells that are not exposed to NPs

and stained with NPs, and B_2 is the cells that are not exposed to NPs and without staining with NPs.

3 Results and discussion

The magnetite SPIONs 9 nm in size and with very narrow size distribution, which was confirmed by transmission electron microscopy (TEM; see Fig. 1), were synthesized by a thermal decomposition method, as described elsewhere.[34] The particles were then coated with carboxyethylsilanetriol (CES) in the presence of DMSO *via* a ligand exchange process.[35,36] The zeta potential of the coated particles was -15.4 ± 0.5. It is worth noting that CES was used as the coating material due to its capability for biomolecular conjugation, which would be essential for further molecular conjugations.[14,37,38] Very recently, we showed that the molecular cellular responses of the three different cell types (*i.e.* 293T (kidney cells), HCM (heart cells) and BE-2-C (brain cells)) to the exact same amounts of SPIONs are different.[39] Here, to probe the responses from individual cells (see Table S1 of the ESI† for details) at the cellular level to the exact same amounts of SPIONs, we employed MTT (3-(4,5-dimethylthiazol-2-yl)-2,5-diphenyltetrazolium bromide)- and XTT (sodium(2,3-bis(2-methoxy-4-nitro-5-sulphophenyl)-2*H*-tetrazolium-5-carboxanilide))-assays, a cell-life cycle assay, an amyloid induction test, and microarrays. It is recommended that for NP toxicity testing, 2 different tests should always be applied;[2] thus, we used both MTT and XTT assays in this research. As shown in Fig. 2, each cell line shows a different cytotoxicity level when treated to the same amount of NPs. More specifically, the same concentration of SPIONs (ranging from 2.25–36 mM) caused significant toxicity on the brain-derived cells (neuronal and glial cells) and lung cells, whereas there was little toxicity on the other cell types. These effects became evident at a concentration of 2.25 mM for neuronal and lung cells, and the cell viability of the glial cells was diminished to less than 80% at particle concentrations of 4.5 mM. The highest SPIONs concentration, 36 mM, is significantly toxic for the majority of the cell lines.

It is well recognized that the physicochemical properties of nanoparticles (*e.g.* material, size and its distribution, shape, surface charge, surface functionalisation, and surface roughness/stiffness) can influence how cells internalize nanoparticles.[13,40] A very recent report shows that the uptake of NPs by cells is influenced by their cell cycle phase;[41] more specifically, the uptake of NPs by the same cells could be ranked according to the different phases: $G_2/M > S > G_0/G_1$. Since the cell population, and the dose of internalized NPs in each cell, can be varied as the cell advances through the cell-life cycle,[41,42] we probed the effect of our nanoparticles on cell-life cycle variation of different cell types. As shown in Fig. 3, the same amount of SPIONs (*i.e.* concentration of 4 mM) caused different responses in the cell cycle of the various cell types. Indeed, the apoptotic fraction (sub G_0G_1 stage) of all SPION-treated cells increased, except for human colon adenocarcinoma cells. Moreover, the amounts of induced apoptosis were significantly different in various cell types. In almost all cell lines, the G_0G_1 phase was reduced and the S phase was prolonged after treatment with the NPs. This may be because the DNA replication characteristic of the S phase was probably required to correct some genetic abnormalities produced by the NP treatment. In addition, the sub G_0G_1 area was increased by NP treatment in almost all cell lines, suggesting the induction of DNA fragmentation and cell apoptosis. The trend is more pronounced in HeLa, HepG2 and L929 cells (see Fig. 3). However, a high sub G_0G_1 area in both treated and untreated cells are seen; thus, this could be a drawback of the entire experiment.

Interestingly, cell cycle analysis shows less sub G_0G_1 peak in 293T and SW480 cells, compared to HepG2. Noting that 293T is of human embryonic kidney origin and that SW489 is a colon cell line, one can explain their cell cycle behavior and resistance based on the notion that these cells are more resistant to toxic agents in food than some other organs of the body.

To further investigate cellular morphological changes of NPs uptake, various cell types (HeLa, L929, and HepG2) were examined using TEM. As shown in Fig. S1 of the ESI,† SPIONs (with average size of around 9 nm) were internalized by the HeLa cells, accumulating inside vesicular structures which might be lysosomes. In addition, the organelle morphology does not seem altered in the presence of SPIONs in the intracellular environment. The TEM images of L929 cells (Fig. S1d and e†) showed that the SPIONs were present in membrane-adjacent multivesicle bodies of micrometer sizes (1–4 μm), entering the cells as larger aggregates than in the HeLa cells. The nuclei and organelles in the control cells remained intact. In order to probe the morphological differences seen in SPION-treated L929 cells, the cells were exposed to crystal violet. As shown in Fig. S1f,† the morphology of damaged cells revealed the presence of gas vesicles inside the cells. Gas vesicles are possibly used to control vertical migration by regulating the gas content and thereby buoyancy. Alternatively, it could be possible that the gas vesicles are used by the cells to position themselves for maximum solar light harvesting. Interestingly, other cell types did not show the formation of gas vesicles.[43] (Fig. S1g–i)† illustrates the broad dispersion of SPIONs in HepG2 intracellular medium. As suggested by the MTT/XTT assays, the SPIONs did not have toxic effects on the HepG2 cells in a wide iron concentration range compared to the other cell types, mainly due to the ability of these cells to handle toxic materials by various metabolic routes.

As shown in Fig. S2 in the ESI,† formation of tight junctions (see Fig. S2a†) and other cellular interactions (see Fig. S2b†) for HepG2 cells are depicted. Although the formation of tight junctions and related morphological characteristics are also formed in the absence of SPIONs, the SPIONs treatment could clearly enhance the cellular interaction leading to the observed characteristics. It could be realized that the observed membrane junctions between HepG2 cells is the unique way that cells were selected to fight with NPs (see Fig. S2c†). It is noteworthy that the morphology of the cells should also be considered for the design of nano-systems; here, the membrane shape of HepG2 cells can simply trap NPs, causing physical aggregation of the NPs.

One of the major responses of proteins to the NPs is aggregation. Both *in vitro* and in the cells, it has been shown that NPs can stimulate protein aggregation.[9,44] In order to examine cell "vision", we exposed a number of cell lines to the same SPIONs, and then measured the level of amyloid formation within the cells. As shown in Fig. 4, the level of Thioflavin T fluorescence, a measure of amyloid formation, was different among the different cell lines examined. Most notably, 293T, HepG2, and Panc1

showed a high level of amyloid induction in the presence of the SPIONs; in contrast, SPIONs had inhibitory effects on amyloid formation in A172, L-929, and HCM cells. Therefore, it can be deduced that in a cell line (293T) derived from kidney, the SPIONs bring about a significantly different response in terms of protein aggregation.

After cellular uptake, the SPIONs commonly reside in endosomes or lysosomes where they are decomposed into free iron and released to the cytoplasm and eventually contribute to the total cellular iron pool. The subsequent fate of iron and its involvement in cell viability and physiology is very complex, and ranges from the stimulation of cell proliferation to variations in the ferritin expression, and ROS production.[45] In order to visualize the lysosome induction caused by SPIONs uptake by various cells, the lysosomes tracker assay was employed on living cells and analyzed by fluorescent microscopy. Fig. 5 shows various amounts of the induced lysosomes after interaction with the same amount of SPIONs. In baseline conditions, the lysosomes seem to be very well represented in Capan-2 cells, followed by Jurkat, Panc-1, and HeLa cells. After incubation with iron, the lysosome formation was strongly induced, this phenomenon was, however, variable among the investigated cell lines, *i.e.* Capan-2 (271%) > Panc-1 (207%) > HeLa (163%) > Jurkat (144%). Knowing that ROS formation is a frequent consequence of SPIONs uptake into late endosomes/lysosomes and subsequent degradation into free iron, confocal microscopy analysis was applied for the selected cells to evaluate the ROS level (see Fig. 5).

The ROS are already produced inside the acidic environment of lysosomes by the reaction of free iron in the form of ferrous ions (Fe^{2+}) with hydrogen peroxide according to the Fenton reaction, resulting thus in the generation of free hydroxide radicals.[45] When it is delivered into the cell, the free iron can cross the nuclear or mitochondrial membrane. The hydrogen peroxide and oxygen produced inside mitochondria react with Fe^{2+}, generating hydroxyl radicals and ferric ions (Fe^{3+}) *via* the Fenton reaction. The hydroxyl radicals could then indirectly damage DNA, proteins and lipids.[46] In agreement with other techniques, various cell types show different ROS level due to their specific selected pathways to fight with NPs. For most of the cells, the ROS production seems to be directly related to the quantity of lysosomes (coefficient of correlation of 0.958) induced by SPION exposure, meaning that Capan-2 cells show the highest ROS generation (340%), followed by Panc-1 (265%) and HeLa cells (118%). The endocrine origin of Capan-2 cells and the associated intense metabolism may explain this prominent SPION uptake (suggested by the induced lysosomes) and the consequent ROS production. This correlation with lysosome content could not be observed in Jurkat cells, where the ROS generation was superior to that in Panc-1 cells (292%). This could be related to the fact that oxidative stress plays an important role in the regulation of the immune system by a precise control of the lymphocytes' survival.[47] Therefore, the ROS production may be a more intense phenomenon in these cells, which must react to death or survival stimuli in a very well controlled manner.

4 Conclusion

Based on the aforementioned results, we conclude that due to their "vision", cells have various ways to handle the NPs; although more investigations should be done to further explore the various responses, we suggest that the preferred route that an individual cell takes constitutes a mapping response just like a "fingerprint" of humans. We have put forward a concept of "cell vision" that can be vital in the bionanosciences. Using several cell lines of different origins, we examined the cellular effects of NPs, *via* various methods (*e.g.* MTT, XTT, cell cycle, ROS, staining, TEM, and microarrays), on different cell types. We suggest that differential inheritance of each cellular component (*i.e.* according to their type) might be much more widespread than is generally appreciated. In order to have deep understanding of "cell vision", there are a number of important questions, which are essential to be answered, as follows:

What are the main detoxification pathways of each type of cells when they comprehend the presence of NPs?

What are the main regulations of cell (*i.e.* specific type of cell) signaling pathways type after treatment with NPs?

How many lysosomes and vesicles are induced in each cell-type after treatment with NPs?

Doing such research on scavenging/detoxifying organelles, in order to define what is the way that each cell type treats NPs?

How cellular components such as mitochondria, endoplasmic reticulum, or Golgi "see" NPs in various cell types?

References

1 M. S. Ehrenberg, A. E. Friedman, J. N. Finkelstein, G. Oberdorster and J. L. McGrath, *Biomaterials*, 2009, **30**, 603.
2 H. F. Krug and P. Wick, *Angew. Chem., Int. Ed.*, 2011, **50**, 1260–1278.
3 ISO/TS: 27687: 2008.
4 A. E. Nel, L. Mudler, D. Velegol, T. Xia, E. M. V. Hoek, P. Somasundaran, F. Klaessig, V. Castranova and M. Thompson, *Nat. Mater.*, 2009, **8**, 543–557.
5 K. A. Dawson, A. Salvati and I. Lynch, *Nat. Nanotechnol.*, 2009, **4**, 84–85.
6 M. Mahmoudi, H. Hosseinkhani, M. Hosseinkhani, S. Boutry, A. Simchi, W. S. Journeay, K. Subramani and S. Laurent, *Chem. Rev.*, 2011, **111**, 253–280.
7 M. P. Monopoli, F. B. Bombelli and K. A. Dawson, *Nat. Nanotechnol.*, 2011, **6**, 11–12.
8 I. Lynch, A. Salvati and K. A. Dawson, *Nat. Nanotechnol.*, 2009, **4**, 546–547.
9 T. Cedervall, I. Lynch, M. Foy, T. Berggerd, S. C. Donnelly, G. Cagney, S. Linse and K. A. Dawson, *Angew. Chem., Int. Ed.*, 2007, **46**, 5754–5756.
10 T. Cedervall, I. Lynch, S. Lindman, T. Berggerd, E. Thulin, H. Nilsson, K. A. Dawson and S. Linse, *Proc. Natl. Acad. Sci. U. S. A.*, 2007, **104**, 2050–2055.
11 M. Mahmoudi, S. Sant, B. Wang, S. Laurent and T. Sen, *Adv. Drug Delivery Rev.*, 2011, **63**, 24–46.
12 S. Laurent, M. R. Ejtehadi, M. Rezaei, P. G. Kehoe and M. Mahmoudi, *RSC Adv.*, 2012, **2**, 5008–5033.
13 M. Mahmoudi, I. Lynch, M. R. Ejtehadi, M. P. Monopoli, F. B. Bombelli and S. Laurent, *Chem. Rev.*, 2011, **111**, 5610–5637.
14 M. Mahmoudi, H. Hofmann, B. Rothen-Rutishauser and A. Petri-Fink, *Chem. Rev.*, 2012, **112**, 2323–2338.
15 S. Sharifi, S. Behzadi, S. Laurent, M. Laird Forrest, P. Stroeve and M. Mahmoudi, *Chem. Soc. Rev.*, 2012, **41**, 2323–2343.
16 I. G. Macara and S. Mili, *Cell*, 2008, **135**, 801–812.
17 H. Summers, *Nano Today*, 2010, **5**, 83–84.
18 N. Lewinski, V. Colvin and R. Drezek, *Small*, 2008, **4**, 26–49.
19 B. Fadeel and A. E. Garcia-Bennett, *Adv. Drug Delivery Rev.*, 2010, **62**, 362–374.
20 N. R. Panyala, E. M. PeMendez and J. Havel, *J. Appl. Biomed.*, 2009, **7**, 75–91.
21 M. V. D. Z. Park, D. P. K. Lankveld, H. van Loveren and W. H. de Jong, *Nanomedicine*, 2009, **4**, 669–685.

22 S. J. H. Soenen and M. De Cuyper, *Nanomedicine*, 2010, **5**, 1261–1275.
23 R. Brayner, *Nano Today*, 2008, **3**, 48–55.
24 P. C. Ray, H. Yu and P. P. Fu, *J. Environ. Sci. Health, Part C: Environ. Carcinog. Ecotoxicol. Rev.*, 2009, **27**, 1–35.
25 M. A. Dobrovolskaia and S. E. McNeil, *Nat. Nanotechnol.*, 2007, **2**, 469–478.
26 R. Hardman, *Environ. Health Perspect.*, 2006, **114**, 165–172.
27 W. H. Suh, A. R. Jang, Y. H. Suh and K. S. Suslick, *Adv. Mater.*, 2006, **18**, 1832–1837.
28 M. R. Wiesner, G. V. Lowry, P. Alvarez, D. Dionysiou and P. Biswas, *Environ. Sci. Technol.*, 2006, **40**, 4336–4345.
29 M. Mahmoudi and V. Serpooshan, *ACS Nano*, 2012, **6**, 2656–2664.
30 M. Mahmoudi, M. A. Sahraian, M. A. Shokrgozar and S. Laurent, *ACS Chem. Neurosci.*, 2011, **2**, 118–140.
31 C. C. Shelton, L. Zhu, D. Chau, L. Yang, R. Wang, H. Djaballah, H. Zheng and Y.-M. Li, *Proc. Natl. Acad. Sci. U. S. A.*, 2009, **106**, 20228.
32 S. J. H. Soenen and M. De Cuyper, *Contrast Media Mol. Imaging*, 2009, **4**, 207–219.
33 J. P. Melchor, L. McVoy and W. E. Van Nostrand, *J. Neurochem.*, 2000, **74**, 2209–2212.
34 J. Park, K. An, Y. Hwang, J.-G. Park, H.-J. Noh, J.-Y. Kim, J.-H. Park, N.-M. Hwang and T. Hyeon, *Nat. Mater.*, 2004, **3**, 891–895.
35 Y. Xu, Y. Qin, S. Palchoudhury and Y. Bao, *Langmuir*, 2011, **27**, 8990–8997.
36 S. Laurent, C. Burtea, C. Thirifays, U. O. Häfeli and M. Mahmoudi, *PLoS One*, 2012, **7**, e29997.
37 G. Subbiahdoss, S. Sharifi, D. W. Grijpma, S. Laurent, H. C. van der Mei, M. Mahmoudi and H. J. Busscher, *Acta Biomater.*, 2012, **8**, 2047–2055.
38 Z. Xu, Q. Liu and J. A. Finch, *Appl. Surf. Sci.*, 1997, **120**, 269–278.
39 M. Mahmoudi, S. Laurent, M. A. Shokrgozar and M. Hosseinkhani, *ACS Nano*, 2011, **5**, 7263–7276.
40 M. Mahmoudi and V. Serpooshan, *J. Phys. Chem. C*, 2011, **115**, 18275–18283.
41 J. A. Kim, C. Aberg, A. Salvati and K. A. Dawson, *Nat. Nanotechnol.*, 2012, **7**, 62–68.
42 M. Mahmoudi, K. Azadmanesh, M. A. Shokrgozar, W. S. Journeay and S. Laurent, *Chem. Rev.*, 2011, **111**, 3407–3432.
43 M. Mahmoudi, A. Simchi, M. Imani, M. A. Shokrgozar, A. S. Milani, U. O. Häfeli and P. Stroeve, *Colloids Surf., B*, 2010, **75**, 300–309.
44 S. Linse, C. Cabaleiro-Lago, W. F. Xue, I. Lynch, S. Lindman, E. Thulin, S. E. Radford and K. A. Dawson, *Proc. Natl. Acad. Sci. U. S. A.*, 2007, **104**, 8691–8696.
45 S. J. H. Soenen and M. De Cuyper, *Contrast Media Mol. Imaging*, 2009, **4**, 207–219.
46 N. Singh, G. J. S. Jenkins, R. Asadi and S. H. Doak, *Nano Rev.*, 2010, **1**, 5358.
47 R. Chiaramonte, E. Bartolini, P. Riso, E. Calzavara, D. Erba, G. Testolin, P. Testolin and G. V. Sherbet, *J. Cell. Biochem.*, 2001, **82**, 437–444.